


AUTHOR QUERY FORM

 ELSEVIER	Journal: Journal of the Mechanical Behavior of Biomedical Materials Article Number: 258	Please e-mail or fax your responses and any corrections to: E-mail: corrections.esch@elsevier.river-valley.com Fax: +44 1392 285879
--	--	---

Dear Author,

Please check your proof carefully and mark all corrections at the appropriate place in the proof (e.g., by using on-screen annotation in the PDF file) or compile them in a separate list.

For correction or revision of any artwork, please consult <http://www.elsevier.com/artworkinstructions>.

Any queries or remarks that have arisen during the processing of your manuscript are listed below and highlighted by flags in the proof. Click on the 'Q' link to go to the location in the proof.

Location in article	Query / remark click on the Q link to go Please insert your reply or correction at the corresponding line in the proof
Q1	Caption of figures 1, 6, 7, 9, 10 and 14 are different in pdf and doc. We have followed pdf. Please check, and correct if necessary.
Q2	Uncited references: This section comprises references that occur in the reference list but not in the body of the text. Please cite each reference in the text or, alternatively, delete it. Any reference not dealt with will be retained in this section.

Thank you for your assistance.

available at www.sciencedirect.comjournal homepage: www.elsevier.com/locate/jmbbm

Research paper

Armadillo armor: Mechanical testing and micro-structural evaluation

Irene H. Chen^a, James H. Kiang^b, Victor Correa^b, Maria I. Lopez^a, Po-Yu Chen^a,
Joanna McKittrick^{a,b}, Marc A. Meyers^{a,b,c,*}

^a Materials Science and Engineering Program, University of California, San Diego, La Jolla, CA 92093, USA

^b Department of Mechanical and Aerospace Engineering, University of California, San Diego, La Jolla, CA 92093, USA

^c Department of Nanoengineering, University of California, San Diego, La Jolla, CA 92093, USA

ARTICLE INFO

Article history:

Keywords:

Armadillo carapace
Mechanical properties
Microstructure
Osteoderm

ABSTRACT

The armadillo has a unique protective bony armor, called the osteoderm, which confers to its shell-like skin distinctive mechanical properties. The top layer of the shell is made out of a dark-brown keratin layer with bimodal size scales. Beneath the keratin layer, the osteoderm consists of hexagonal or triangular tiles having a composition that is the same as bone. The tiles are connected by non-mineralized collagen fibers, called Sharpey's fibers. The tough and highly mineralized tiles have a tensile strength of approximately 20 MPa and toughness of around 1.1 MJ/m³. In comparison, the hydrated osteoderm has a lower tensile strength of ~16 MPa and a toughness of 0.5 MJ/m³. The tensile failure occurs by the stretching and rupture of the Sharpey's fibers. In a specially designed punch test in which an individual tile is pushed out, the shear strength is ~18 MPa, close to the tensile strength of the osteoderm. This surprising result is interpreted in terms of deformation in the Sharpey's fibers in the hydrated condition. The armadillo shell and a turtle shell are compared, with their corresponding similarities and differences.

© 2010 Elsevier Ltd. All rights reserved.

1. Introduction

There are approximately twenty species of armadillo, ranging from 0.15 to 1.5 m in length. The most common one found in the US is the nine-banded armadillo, *Dasypus novemcinctus* (Weiss and Wislocki, 1956; Gardner et al., 2005). Its average length is 0.75 m (including the tail) and average weight is 6 kg. The armadillo carapace is divided into five different regions: the head, pectoral, banded, pelvic shields and tail (Fig. 1(a)). The entire top layer of the carapace is covered

with a dark brown keratin layer (Fig. 1(b)). Beneath the keratin layer, a well organized arrangement of bony tiles is closely compacted together and connected by collagen fibers (Fig. 1(c)). These collagen fibers, also called Sharpey's fibers, are non-mineralized and hold the tiles together; they diverge from the center of the tile element (Vickaryous and Hall, 2006). The tiles demonstrate two phenotypes depending on the region where they are located. They are hexagonally shaped in the pectoral and pelvic regions and have triangular structures along the mid-section of the body (Fig. 1(b) and (c)).

* Corresponding author at: Materials Science and Engineering Program, University of California, San Diego, La Jolla, CA 92093, USA. Tel.: +1 858 534 4719; fax: +1 858 534 5698.

E-mail address: mameyers@ucsd.edu (M.A. Meyers).

1751-6161/\$ - see front matter © 2010 Elsevier Ltd. All rights reserved.

doi:10.1016/j.jmbbm.2010.12.013

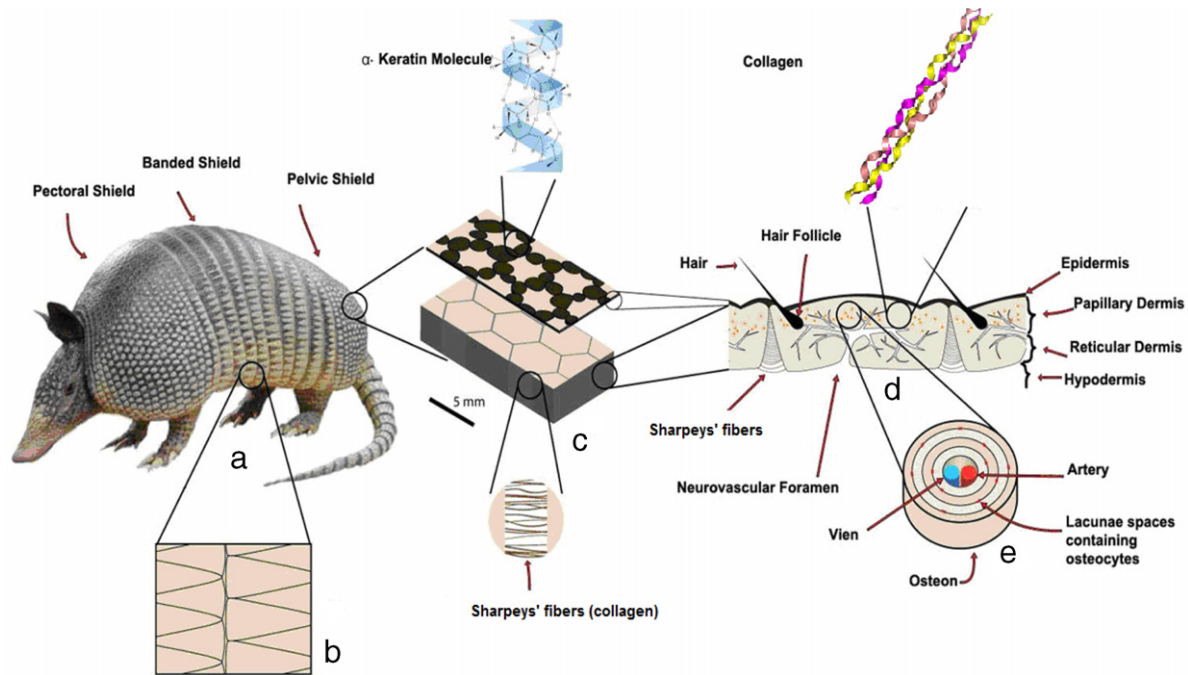


Fig. 1 – Hierarchical structure of the armadillo carapace: (a) whole body; (b) triangular tile (in the banded shield); (c) hexagonal tile with top layer of keratin (exploded view); (d) cross-sectional view of the carapace (osteoderm and Sharpey's fibers).

1 Within the cross-sectional view of the tiles, four different
 2 layers are observed, from exterior to interior: epidermis,
 3 papillary, reticular, and hypodermis (Fig. 1(d)) (Vickaryous and
 4 Hall, 2006). The epidermis is composed of keratin and plays
 5 only a minor role in protection against mechanical forces.
 6 The papillary dermis is composed mostly of a type I collagen
 7 fiber network and laterally oriented osteons (Fig. 1(e)), with
 8 blood vessels channeling from the bottom hypodermis layer
 9 and providing nutrients (Vickaryous and Hall, 2006). The
 10 osteon is the fundamental basic unit of cortical bone and is
 11 identified as a central vascular canal wrapped with concentric
 12 lamellae, each composed of oriented mineralized collagen
 13 fibrils. Within the concentric lamella are evenly distributed
 14 osteocyte lacunae. The reticular dermis layer is characterized
 15 by a large amount of porosity and the bottom hypodermis
 16 layer has a sheath of collagen matrix surrounded by blood
 17 vessels (Hill, 2006; Vickaryous and Hall, 2006).

18 Fig. 2(a) shows the arrangement of epidermal keratin
 19 scales, showing a bimodal distribution consisting of large
 20 bright regions, which are surrounded by smaller dark regions.
 21 The modeling of the bimodal distribution of the number
 22 of cell sides using numerical methods and topological
 23 properties was performed by Parfait-Pignol et al. (1998) on
 24 armadillo scales. They defined the edge number distribution
 25 as: $p(n) = \alpha p_1(n) + (1 + \alpha)p_2(n)$, where $p(n)$ is the edge
 26 number distribution normalized to 1 for each i , and $\langle n \rangle_i$
 27 is the mean number of edges of cells which belong to class i :
 28 $\langle n \rangle_i = \sum_n n p_i(n)$. A simplified analysis was applied here and
 29 is shown in Fig. 2(b). The bimodal distribution is clearly seen
 30 and in agreement with the Parfait-Pignol et al. (1998) analysis
 31 of the keratin scales on the armadillo. There are two peaks:
 32 $n = 8$ (for the large bright scales) and $n = 5$ (for the smaller

dark scales), compared with Parfait-Pignol's analysis, which
 resulted in two peaks at $n = 7.2$ and $n = 4$. It is important to
 point out that the bony layer does not reproduce the bimodal
 scale distribution of the keratinous layer; there is no direct
 correspondence between the scales and tiles.

The carapace can have a varying curvature and this is
 enabled by the structure composed of tiles and Sharpey's
 fibers. The stretched state (Fig. 3(a)) and the curved state
 (Fig. 3(b)) are accompanied by extension and retraction of
 Sharpey's fibers, respectively. The outer dimensions (D_1)
 of the tiles are greater than the inner dimensions (D_2). The
 curved configuration represents a typical armadillo carapace
 in nature. The length of the Sharpey's fibers can be varied to
 give the entire carapace structure the desired curvature.

Most studies on the armadillo focus on the histology
 and developments on the osteoderm. The formation of the
 osteoderm is a fairly delayed process compared to the rest
 of the skeleton of the body (Vickaryous and Hall, 2006). The
 osteoderm represents a relatively robust foundation upon
 which to base soft-tissue reconstructions of extinct xenarthrans
 (Hill, 2006). Studying armadillo osteoderms allows a more
 in-depth understanding of bone reconstruction (Weiss and
 Wislocki, 1956).

Recently, biomimetic designs have drawn great attention
 from the Materials Science community. There are other
 examples of pre-biomimetic applications in history using
 tiled arrangements, such as the Roman testudo and Japanese
 armor. A tight arrangement of hexagonal tiles can be very
 strong due to the densely compacted morphology. Our
 suggestion is that the armadillo osteoderm could have
 unique mechanical properties which serve seemingly as a
 protective armor against predators' claws and teeth. So far,

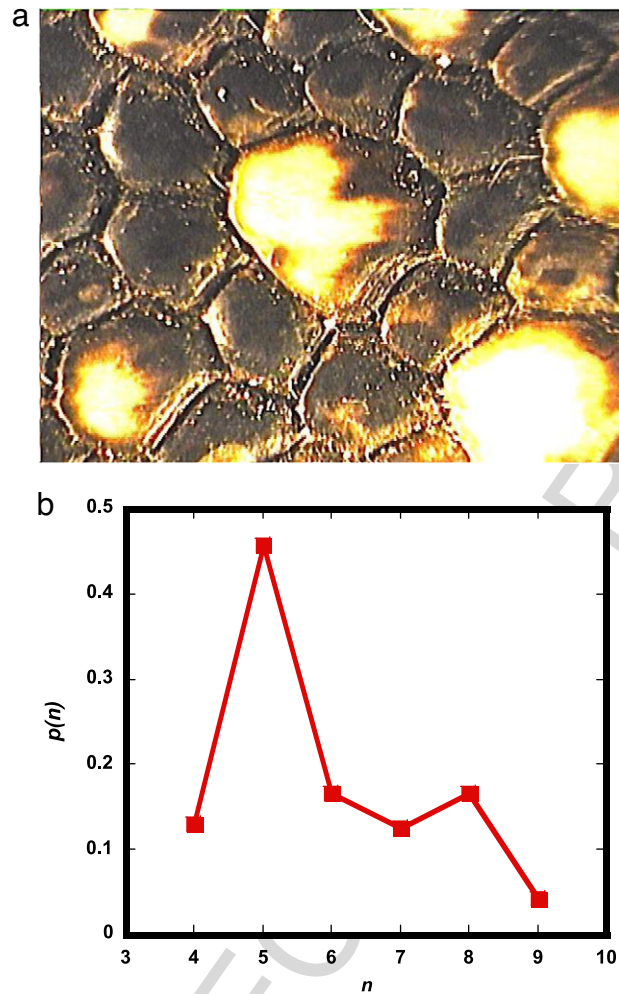


Fig. 2 - Surface of the shell (keratin layer) showing the bimodal distribution of scales with larger (light) scales surrounded by smaller (dark) scales; (b) edge number distribution $p(n)$ vs number of edge cells n with the small cells $\alpha = 0.74$ peak at $n = 5$ and $p(n) = 0.45$.

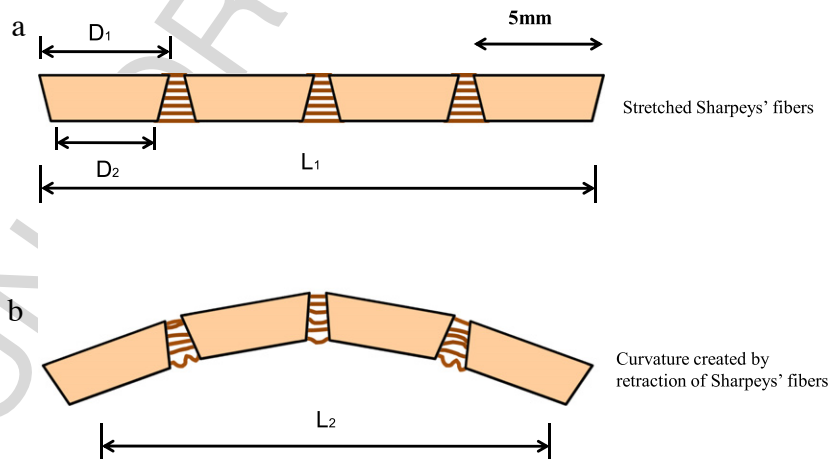


Fig. 3 - Cross-sectional morphology of osteoderm scales of stretched vs curved carapace ($D_1 > D_2$). The retraction of Sharpey's fibers creates a variable curvature.

1 there have been no studies on the mechanical properties of its microstructure and mechanical properties in order to 3
 2 achieve an improved understanding of the protection that the 4



Fig. 4 – Osteoderm after heating in a furnace to 550 °C for 24 h. The organic substance and water were baked off, leaving only the mineral phase.

carapace offers, in a similar manner to the recent study on the armored scales of a fish (Bruet et al., 2008).

2. Materials and methods

Five individual hexagonal shaped armadillo tiles each weighting ~1.5 g and taken from the pectoral and pelvic shields of the armadillo carapace (Jernigan's Taxidermy, Waco, Texas) were used in determining the water and ash contents. Samples were dried in a muffle furnace at 105 °C for 12 h and the dry weights were measured using a balance. Samples were then ashed at 550 °C for 24 h and ash weights were measured. The water content (in wt %) was calculated by dividing the difference between the ambient weight and furnace-dried weight by the ambient weight and the mineral

content (in wt %) was calculated by dividing the ashed weight by the furnace-dried weight of the samples.

X-ray diffraction (XRD) was performed on the powder from ground armadillo shell specimens using a bench top XRD system (MiniFlex™ II, Rigaku Company, Austin, Texas). The scan was performed continuously from $2\theta = 20^\circ$ to 60° , with a step size of 0.01° at a rate of $1^\circ/\text{min}$. The radiation source was $\text{CuK}\alpha_1$ with a wavelength of 0.154 nm.

X-ray fluorescence (XRF) (Horiba XGT-5000, Irvine, California) with an X-ray tube energy 30 kV was used to identify the location of calcium in the sample. The samples for analysis were cut from the pelvic region of the tiles into 1.5 cm squares and placed under an X-ray beam of diameter 100 μm .

The dried armadillo osteoderm specimens were cut into dumbbell shapes with dimensions: gauge length 12 mm, width 7.2 mm, and thickness 2.60 mm. The specimens were cut using a LaserCMM™ (Hayward, CA) and tested in a 500 N universal testing system (Instron 3342, Norwood, MA) at a strain rate of 10^{-3} s^{-1} . Ten hydrated (in distilled water for 24 h) and ten dry (ambient) samples were tested under tensile load. The fracture surface was characterized using scanning electron microscopy (SEM) (Phillips XL30SEM, Hillsboro, Oregon). The samples were subsequently sputter coated with carbon prior to SEM imaging. Cross-sectional samples prepared for optical microscopy were mounted in epoxy, followed by grinding and polishing. Optical micrographs were taken using a Zeiss Axio imager (Zeiss MicroImaging Inc., Thornwood, NY, USA) equipped with a CCD camera.

The shear tests were conducted in the same tensile testing machine by using a hexagonal punch with a radius of 2.69 mm, smaller than the tiles, on the pectoral surface of the osteoderm. The bottom part consisted of a circular ring with a central orifice slightly larger than the punch and larger than the tile. The sample was sandwiched between the punch and the ring; the samples were tested in the hydrated condition at a strain rate of $2 \times 10^{-2} \text{ s}^{-1}$.

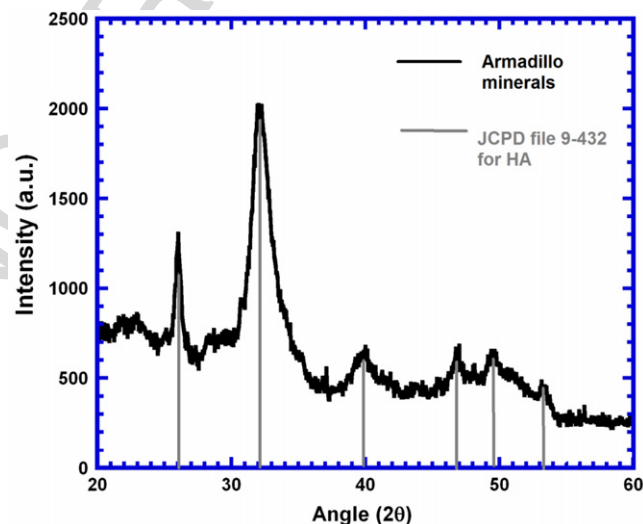


Fig. 5 – X-ray diffraction results of the crushed air dried armadillo carapace. The pattern indexes to JCPDS file 9-432 for hydroxyapatite.

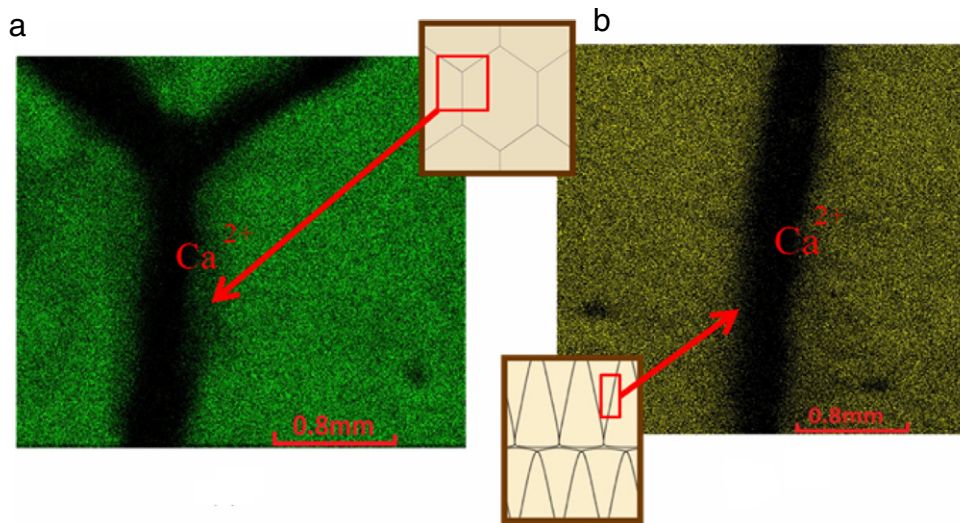


Fig. 6 – X-ray fluorescence images taken on (a) the hexagonal tiles. The bright green color corresponds to calcium. Calcium is not found between the tiles, indicating that Sharpey's fibers are not mineralized and, (b) same for rectangular tiles. These images also show a high calcium concentration in the tiles and little or no calcium between the tiles.

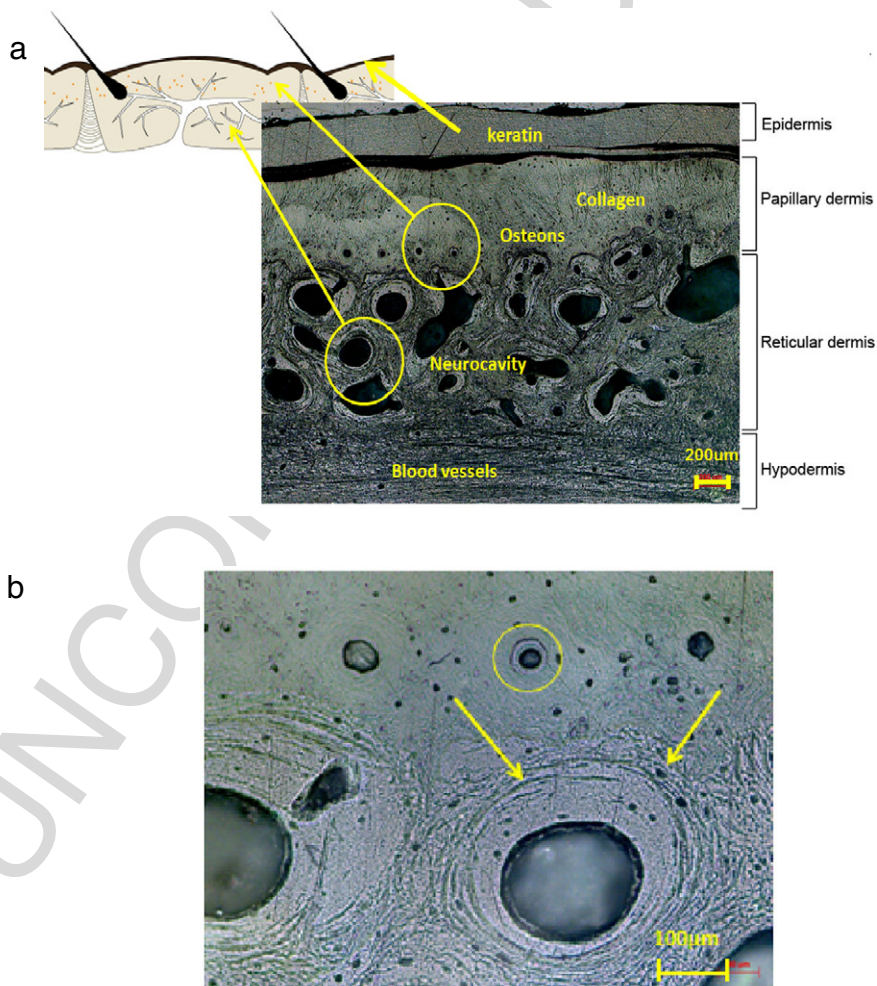


Fig. 7 – (a) Optical microscope image of the osteoderm cross section showing osteons and the porous region and (b) image of large osteons (circle) and pores (arrow) which are surrounded by lacunae spaces.

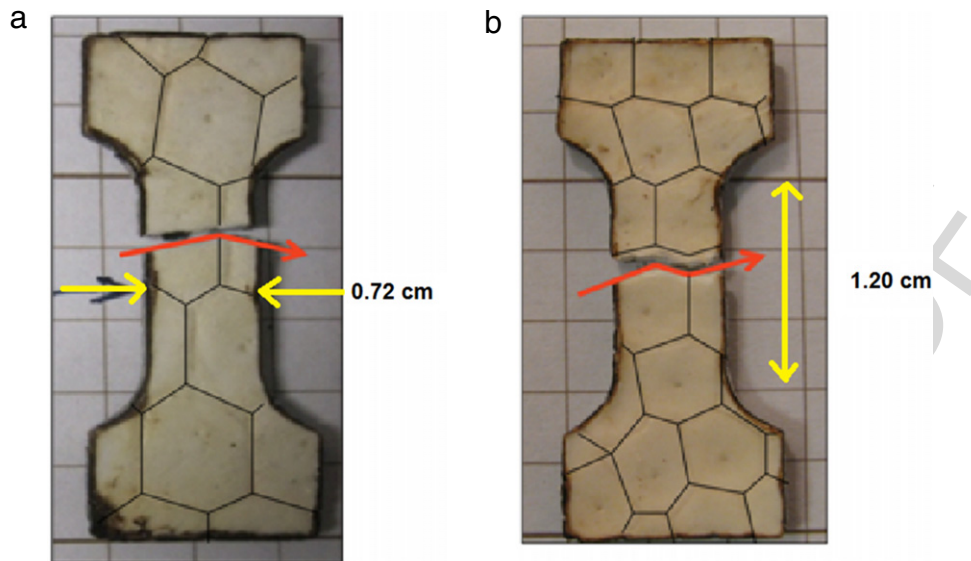


Fig. 8 – Osteoderm failure mechanisms: (a) trans-tile (dry) and (b) inter-tile (hydrated).

3. Results and discussion

Based on the drying and ashing experiments, the hexagonal tiles have 13.6 ± 0.4 (wt%) water and 64.8 ± 1.3 (wt%) mineral. The remainder of the material besides the mineral and water are the inorganic components: collagen and keratin. The organic protein components in Fig. 4 have been baked off, leaving only the mineral phase content, showing that the mineral constituents are distributed uniformly throughout the tiles.

The XRD pattern of air dried, ground tiles is compared with hydroxyapatite. Fig. 5 shows that the osteoderm mineral has the same crystal structure as hydroxyapatite according to JCPDS for hydroxyapatite (File 9-432). XRF mapping from Fig. 6(a) and (b) confirmed that hexagonal and rectangular tiles are calcium rich, whereas the junction (location of the Sharpey's fibers) between the tiles have little or no calcium, confirming that the Sharpey's fibers are non-mineralized.

The optical microscope image in Fig. 7(a) reveals the cross-sectional view of a typical armadillo osteoderm corresponding to the cartoon image on the left side. The keratin component on the top epidermis layer is approximately $120 \mu\text{m}$ thick, followed by the thicker papillary layer ($350 \mu\text{m}$) composed of a dense collagen fiber matrix. Several small hollow spaces with layers of concentric lamellae of diameters $120\text{--}150 \mu\text{m}$ are found at the bottom of papillary; they correlate to osteons with vascular channels ranging from 10 to $15 \mu\text{m}$. There are evenly distributed lacunae spaces of diameter $10 \mu\text{m}$ found both surrounding and internal to these osteons. The armadillo osteons are slightly smaller than those of bovine femur bone ($\sim 200 \mu\text{m}$). The collagenous high porosity region (reticular dermis layer) has larger cavities, with diameters of $100\text{--}400 \mu\text{m}$, along with some evenly distributed lacunae spaces of $10 \mu\text{m}$. These cavities are believed to be secondary osteons resulting from bone remodeling. In the hypodermis layer, limited traces of blood

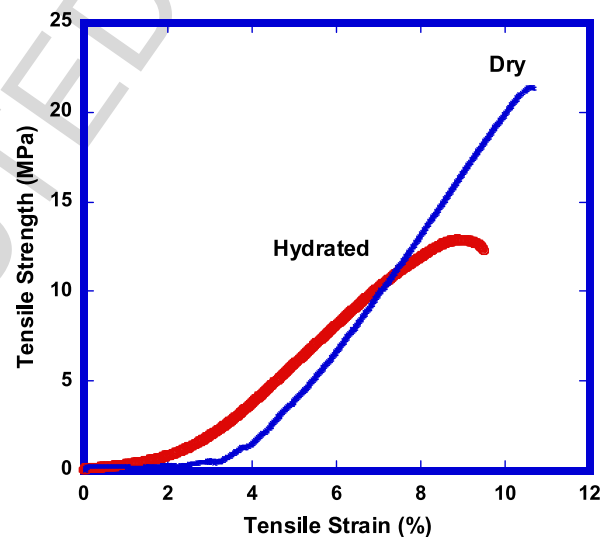


Fig. 9 – Representative stress–strain tensile relationships of dry and hydrated samples. The dry sample suffered fracture through the tile (trans-tile) whereas the hydrated sample suffered fracture between the tiles (inter-tile), along the Sharpey's fibers.

vessels were observed which are oriented parallel to the surface. Fig. 7(b) shows the osteons (circle) and cavities. The large cavities (arrow) are surrounded by lacunae spaces and there are smaller osteons located directly above the large cavities.

Two types of tensile failure were observed in the samples: trans-tile (Fig. 8(a)) and inter-tile (Fig. 8(b)). The inter-tile fracture was usually found in the hydrated samples, in contrast to the trans-tile fracture that was normally found in the dry samples. The dry samples had a higher tensile strength and Young's modulus than the hydrated samples, as shown in Fig. 9 (representative specimens). The Young's modulus was taken between tensile strains of 4% and 8% for the

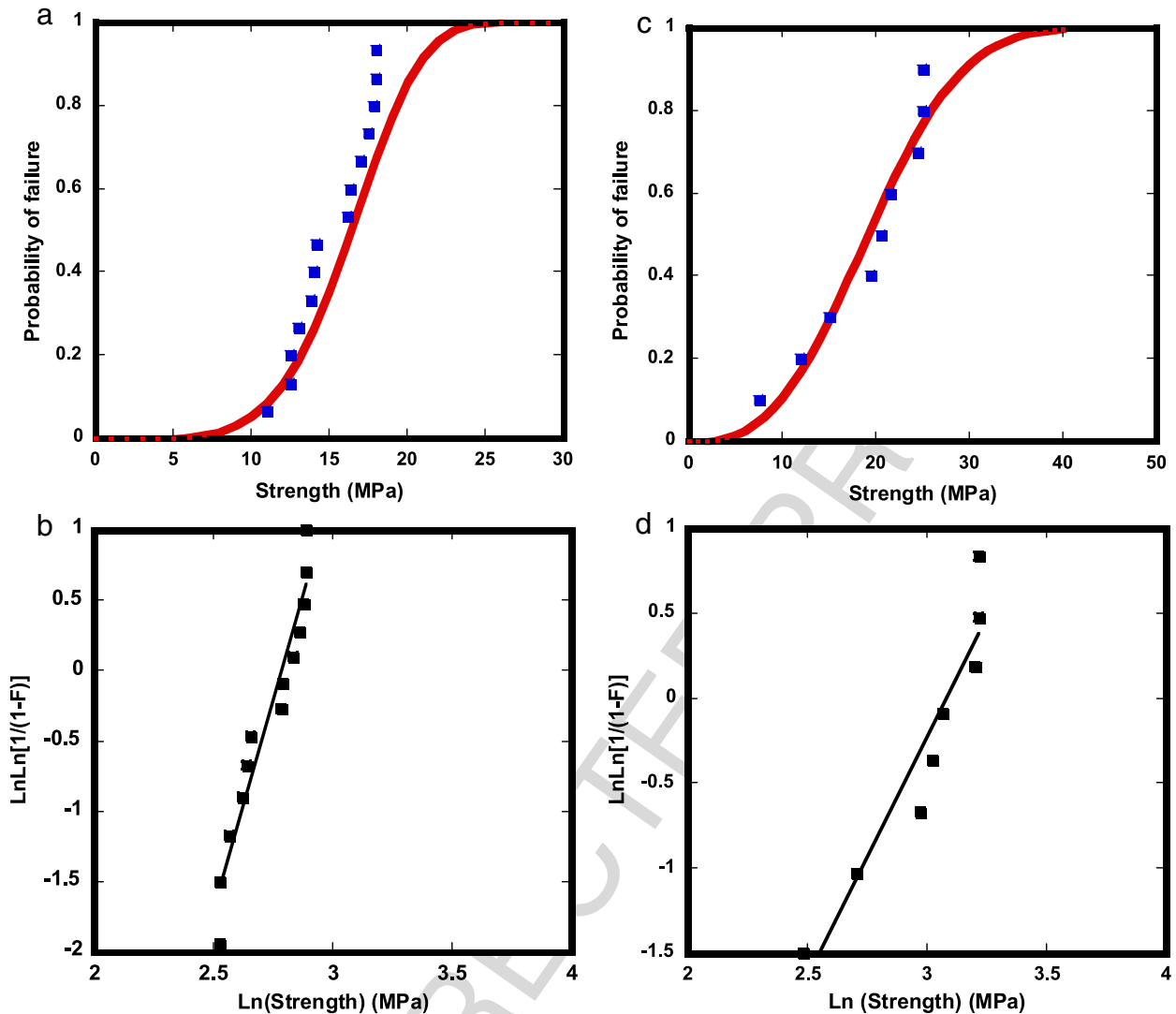


Fig. 10 – (a) Weibull distribution results from tensile tests of hydrated samples with probability of failure at 50% = 16 MPa; (b) Weibull plot with modulus $m = 5.93$. F is defined as the failure probability. (c) Weibull distribution results from tensile tests of dry samples with probability of failure at 50% = 20 MPa. (d) Weibull plot for obtaining $m = 2.80$.

Table 1 – Mechanical properties (Young's modulus, tensile strength, toughness) of dry and hydrated armadillo osteoderm samples (ten of each condition).

Material	Young's modulus (MPa)	Tensile strength (MPa)	Toughness (MJ/m ³)	Reference
Turkey tendon ^a (14 months)	214 ± 98	44 ± 14	2.2 ± 0.2	Silver et al., 2000
Armadillo osteoderm (wet)	150 ± 25	13 ± 5	0.53 ± 0.1	This work
Armadillo osteoderm (dry)	425 ± 30	23 ± 5	1.10 ± 0.1	This work
Bovine femur ^b	19,400 ± 1000	142 ± 20	1.75 ± 0.25	Martin et al., 1998

^aTurkey tendon with 14 weeks of mineralization has an mineral content of 29.5 wt %.

^bBovine femur has an mineral content of 66–67 wt %.

dry samples and between 2% and 6% for the hydrated samples. The dry and hydrated toughness values were calculated from the areas below the stress-strain curves. The samples with a trans-tile fracture showed a higher tensile strength than samples with inter-tile fracture. Table 1 lists the average Young's modulus, tensile strength and toughness for dry samples (with 71% trans-tile failure) and hydrated samples

(with 86% inter-tile failure); for comparison purposes, bovine bone and turkey tendon properties are also given. The Young's moduli (dry = 425 MPa, hydrated = 150 MPa) are given in comparison with bovine femur (19.4 GPa) and turkey tendon (214 MPa). Young's modulus for the dry and wet osteoderm are respectively higher and lower than that for turkey tendon. Both the dry and wet osteoderm have much lower modulus

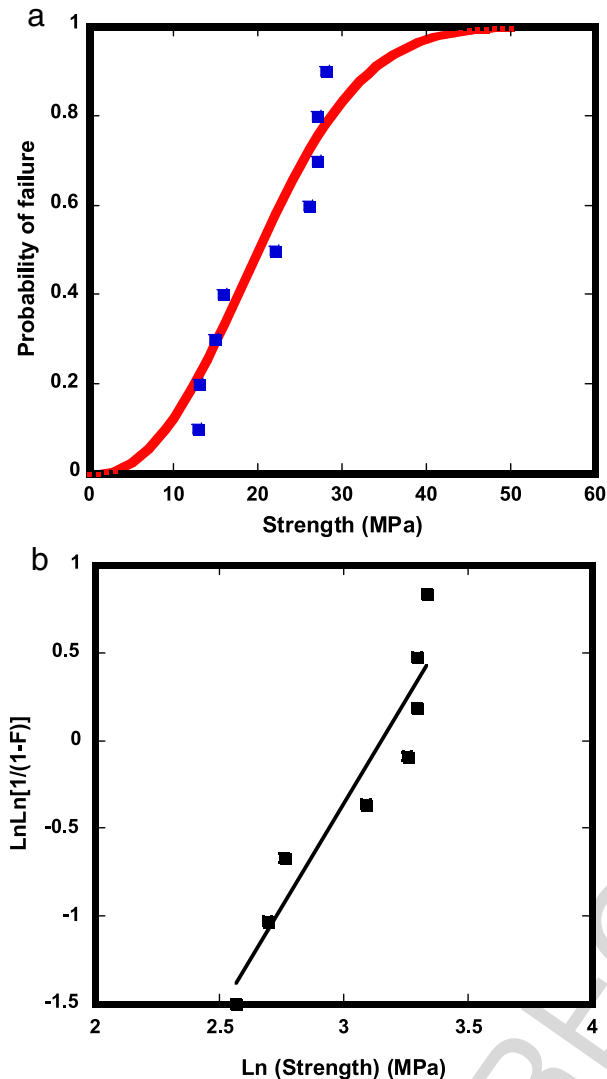


Fig. 11 – (a) Weibull distribution results from shear tests of hydrated samples, probability failure at 50% = 18 MPa; (b) Weibull plot obtaining $m = 2.35$.

values than bovine femur. The tensile strength (dry, 23 MPa) is lower than that of the bovine femur but both have comparable toughness values. The tensile strength (hydrated, 13 MPa) is also lower than that of turkey tendon (44 MPa); the hydrated condition has a lower toughness (0.53 MJ/m^3). The differences between the dry and hydrated conditions can be explained by the effect of hydration on collagen. Hydrated collagen is more flexible and softer; therefore most of the deformation occurs on the Sharpey's fibers. On the other hand, in the dry specimens failure occurs in the mineralized tiles in a more brittle manner.

Weibull statistical analysis of tensile test results was performed on the hydrated (Fig. 10(a) and (b)) and dry (Fig. 10(c) and (d)) specimens. The basic assumption for Weibull analysis is that the samples have non-interacting flaws (e.g., Meyers and Chawla, 2009). The plots used to obtain m are shown in Fig. 10(b) and (d). The Weibull modulus, m , which is the measure of the variability of the strength of the shell, was found to be 5.93 for the hydrated and 2.80

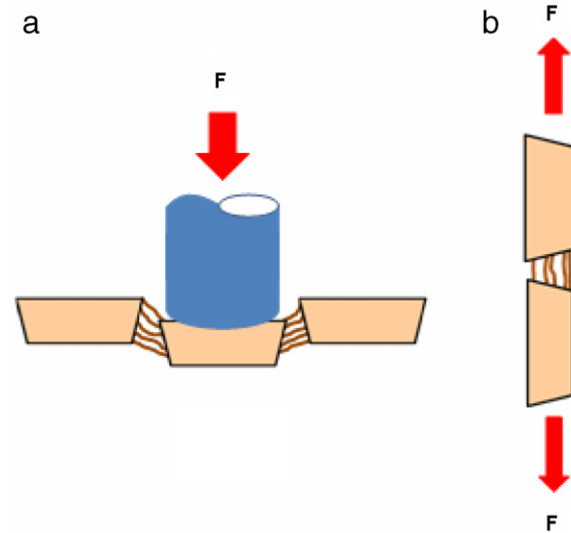


Fig. 12 – Schematic diagram of the (a) shear test and (b) tensile test configurations.

for the dry samples. The m values are the slopes taken from the double-natural-logarithmic plots. F is defined as the failure probability. The values for m fall in the category of biological materials (and whiteware ceramics), which show great variability of strength (Meyers and Chawla, 2009). The stress with 50% probability of failure (taken as the average strength) is 16 MPa for the hydrated samples and 20 MPa for the dry samples. The shear strengths, determined by using the punch test, are shown in Fig. 11(a). The corresponding plot to obtain the Weibull distribution is given in Fig. 11(b). The values predicted were around 18 ± 3 MPa. Fig. 12 shows schematically how the shear (Fig. 12(a)) and tensile (Fig. 12(b)) tests subject the Sharpey's fibers both to tensile loading. This is why similar values are obtained for the tensile and shear strengths. In isotropic monolithic materials, on the other hand, the shear strength is one half the tensile strength.

The SEM image in Fig. 13(a) shows several osteons on a fracture surface after tensile testing of a dry sample. This indicates that the fracture occurred on the mineralized tiles where the osteons are located. In Fig. 13(b), the image shows densely packed, concentrically oriented mineralized collagen fibers surrounding the vascular channels. Fig. 13(c) and (d) are SEM images comparing collagen fibers of mineralized (found on the tiles) and non-mineralized (found on Sharpey's fiber) types. Fig. 13(c) shows that the Sharpey's fiber has a smooth surface, and Fig. 13(d) shows a mineralized collagen fiber that is found in the tile bone.

It is interesting to compare the structure and properties of the armadillo armor with those of the turtle shell (both dorsal-carapace and ventral-plastron). They perform similar functions – protection from predators – and the structures show some similarity. One distinction is that in turtles the dorsal shell contains the vertebrae and ribs (Fig. 14(a)); however, these are located inside the armadillo and totally separated from the shell (Krauss et al., 2009). The tiles of the turtle contain a significant amount of porosity, shown in Fig. 14(b) for a Red ear turtle. The carapace and plastron of turtles are composed of separate interconnected bone

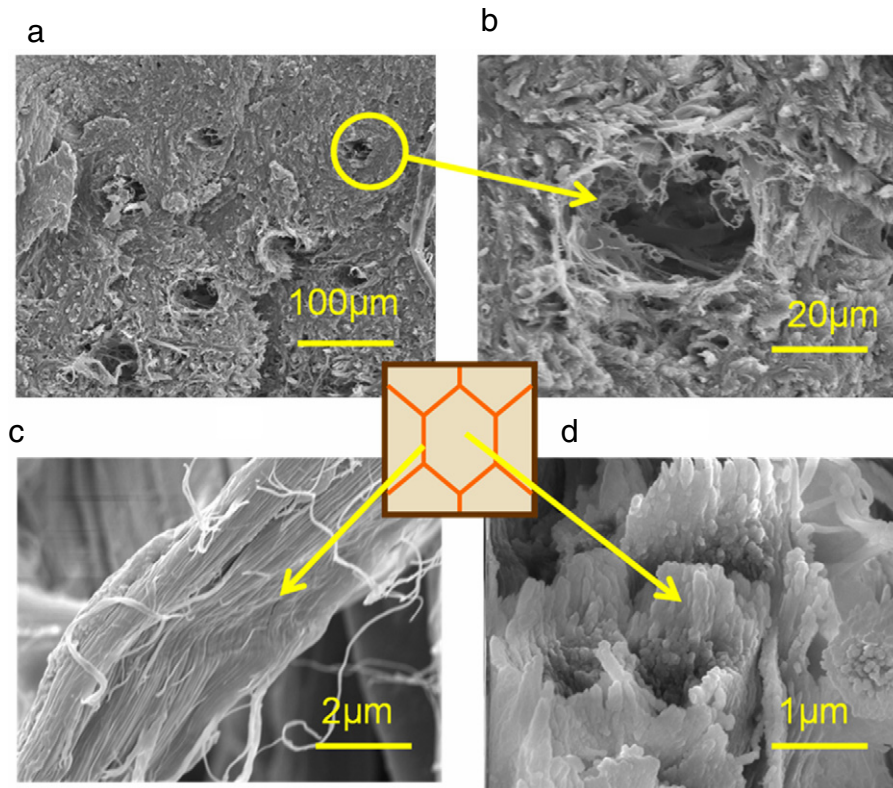


Fig. 13 – SEM micrographs of the fracture surface of the osteoderm. (a) Cross-sectional view of osteons in the papillary dermis; (b) Higher magnification view of the osteon of $\sim 50\ \mu\text{m}$ in diameter surrounded by a dense collagen network; (c) non-mineralized Sharpey's fibers; (d) mineralized collagen fibers on the bony portion of the tile.

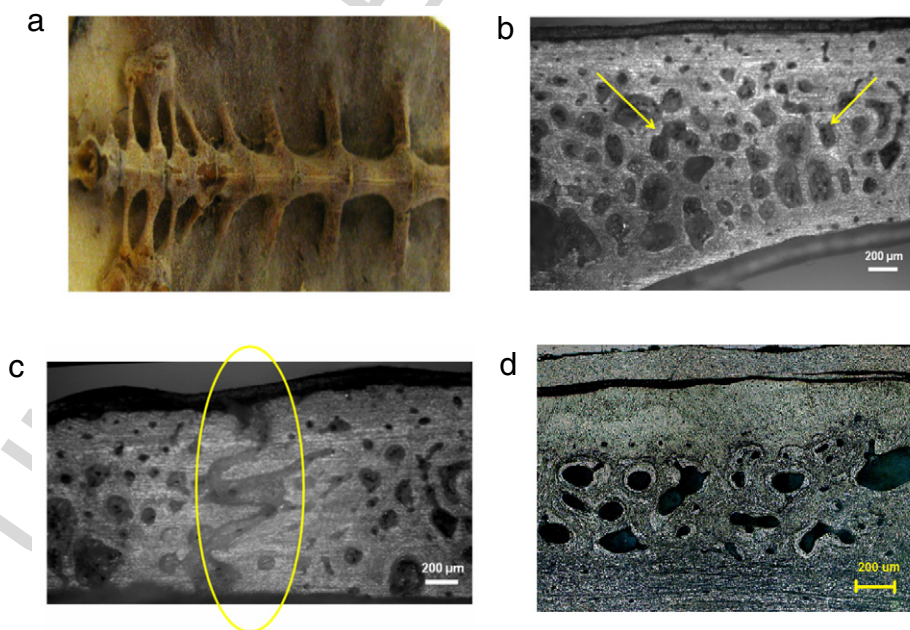


Fig. 14 – (a) Inside view of turtle carapace showing fused vertebrae and ribs; (b) section of plastron showing porous cavities; (c) section of plastron showing the suture between two plates (marked in the figure); (d) cross-sectional view of the armadillo shell showing a porous region similar to turtle plastron.

(Rhee et al., 2009), similar to the armadillo. Thus, there is some flexibility of the shell, especially at low strain rates (Krauss et al., 2009); at high strain rates the shell becomes rigid. The material between bony plates in turtle shells, called a suture, is also non-mineralized collagen. The structure of the sutures is more complex than the inter-tile region in the armadillo. They have a 'zigzag' geometry that provides much greater local protection than the Sharpey's fibers in the armadillo (Fig. 14(c)). Fig. 14(d) demonstrates a porous structural comparison of the cross-sectional view of the armadillo armor and turtle plastron. It confirms the porous structural similarities between the armadillo and turtle. There is also very interesting turtle that has a carapace consisting, like armadillo, of osteoderms: the leatherback. Its most notable feature is the lack of a bony carapace; it has a thick leathery skin with embedded osteoderms. Since the armadillo and leatherback turtle belong to two different families, mammals and reptiles, respectively, it is fascinating that evolutionary convergence led to similar solutions for protection from predators.

4. Conclusions

The armadillo armor is a composite material consisting of hard mineralized tiles connected by soft non-mineralized collagen fibrils (Sharpey's fibers). This structure gives the shell mechanical properties between hard and soft tissue. The mineralized tiles of the armadillo shell have a competitive mechanical advantage over the keratin of predators' claws and teeth. The tensile strength for the dry mineralized tiles (~20 MPa) is higher than the strength of the non-mineralized Sharpey's fibers in the hydrated condition (~16 MPa). Both of these values are lower than the tensile strength of mineralized turkey tendon and bovine femur bone. The osteoderm showed a much higher toughness in comparison to the turkey tendon. The results of tensile tests (16 MPa) and shear tests (18 MPa) show that these values are quite close — in both cases tensile failure of the Sharpey's fibers occurred.

Uncited references

Meyers et al., 2008.

Acknowledgements

This research is supported by the National Science Foundation, Division of Materials Research, Ceramics Program Grant 1006931 and Biomaterials Program Grant 0510138. We thank Ryan Anderson (CalIT²) and Maribel Montero (CalIT²) for help with SEM and XRF, Steve Lee (UC San Diego) for schematic drawing, and Joshua K. Yee (UC Irvine) for sample preparation.

REFERENCES

- Bruet, B.J.F., Song, J., Boyce, M.C., Ortiz, C., 2008. Materials design principles of ancient fish armor. *Nat. Mater.* 7, 748–758.
- Gardner, A., Wilson, D.E., Reeder, D.M., 2005. *Mammal Species of the World*, 3rd ed.. Johns Hopkins University Press, 94–99.
- Hill, R.V., 2006. Comparative anatomy and histology of xenarthan osteoderms. *J. Morph.* 267, 1441–1460.
- Krauss, S., Monsonogo-Ornan, E., Zelzer, E., Fratzl, P., Shahar, R., 2009. Mechanical function of a complex three-dimensional suture joining the bony elements in the shell of the red-eared slider turtle. *Adv. Mat.* 21, 407–412.
- Martin, B.R., Burr, D.B., Sharkey, N.A., 1998. *Skeletal Tissue Mechanics*. Springer, New York, 164–165.
- Meyers, M.A., Chawla, K.K., 2009. *Mechanical Behavior of Materials*, 2nd ed.. Cambridge University Press, 79–80.
- Meyers, M.A., Chen, P.-Y., Lin, A.-Y., Seki, Y., 2008. Biological materials: structure and mechanical properties. *Prog. Mater. Sci.* 53, 1–20.
- Parfait-Pignol, V., Le Caër, G., Delannay, R., 1998. On some natural and model 2D bimodal random cellular structures. *Eur. Phys. J.* 4, 499–511.
- Rhee, H., Horstemeyer, M.F., Hwang, Y., Lim, H., El Kadiri, H., Trim, W., 2009. A study on the structure and mechanical behavior of the *Terrapene carolina* carapace: a pathway to design of bio-inspired synthetic composites. *Mater. Sci. Eng. C* 29, 2333–2339.
- Silver, F.H., Chritansen, D., Snowhill, P.B., Chen, Y., Landis, W.J., 2000. The role of mineral in the storage of elastic energy in turkey tendons. *Biomacromol* 1, 180–185.
- Vickaryous, M.K., Hall, B.K., 2006. Osteoderm morphology and development in the nine-banded armadillo, *Dasypus novemcinctus* (Mammalia, Xenathra, Cingulata). *J. Morph.* 267, 1273–1283. 2006.
- Weiss, L.P., Wislocki, G.B., 1956. Seasonal variations in hematopoiesis in the dermal bones of the nine banded armadillo. *Anat. Rec.* 2, 143–163.